Removing Error Floor for Bit Interleaved Coded Modulation MIMO Transmission with Iterative Detection

Alexander Boronka, Nabil Sven Muhammad and Joachim Speidel
Institute of Telecommunications, University of Stuttgart
Pfaffenwaldring 47, D-70569 Stuttgart, Germany
Tel.: +49 711 685 7945 Fax: +49 711 685 7929
e-mail: {boronka,muhammad,speidel}@inue.uni-stuttgart.de

***Abstract*— We present a method to remove the error floor of an iterative bit interleaved coded modulation MIMO (multiple-input multiple-output) system when Gray mapping is used without shifting the position of the turbo cliff to higher SNR. To do so code doping is applied by introducing an additional rate 1 inner encoder. We optimize doping rate and outer code by using the EXIT chart. Simulations reveal transmission without error floor for a rate $1/2$, 4×4 MIMO system with 16-QAM per antenna, resulting in a transmission of 8 information bits per channel use, with a turbo cliff position that is 2 dB smaller compared to state of the art.**

***Index Terms*— MIMO, MMSE, BICM, iterative decoding, turbo decoding, code doping**

I. Introduction

In the last years, intensive research was done on anti-Gray mappings. This was motivated by the fact that they can iteratively decrease the bit error ratio (BER) when used as an inner rate 1 encoder of a serially concatenated coding scheme [1], [2]. The demapper is used as inner decoder in a turbo receiver, which iteratively exchanges extrinsic information with the outer a posteriori probability (APP) decoder.

The principle of bit interleaved coded modulation (BICM) given in [3] can be improved by iterative detection. However, the performance mainly depends on two points: First, in the EXIT chart [4], [5] the transfer characteristic $I_E(I_A)$ of the demapper has to reach a high value for perfect a priori information. In other words the end value $I_E(I_A=1)$ must be high. Secondly, the transfer characteristics of the demapper and the decoder have to match in such a way that they build up a tunnel, even for low signal to noise ratio (SNR). The first condition is relatively easy to meet. Methods to fulfill the second requirement are under current research. It is well known that if the end point $I_E(I_A=1)$ of the demapper transfer characteristic is high, its starting point $I_E(I_A=0)$ is lowered, because the area under the curve is constant [6]. This leads to an early intersection of the characteristics of the demapper and the decoder, resulting in a turbo cliff at an unfavorable high SNR.

If the intersection point of the two transfer characteristics is not close to $(I_A=1, I_E=1)$, then a serious BER floor results, which cannot be reduced by further iterations. A method to remove this error floor without introducing additional redundancy was presented in [7] for multicarrier CDMA systems using a heavy punctured inner code, which is also called code doping. Recently, this technique was combined with OFDM [8]. For a low complexity MIMO system with 4 transmit and 4 receive antennas, applying 16-QAM and an outer code of rate $1/2$ an impressive error floor free transmission with a turbo cliff at about 8 dB was achieved in [9].

In this paper we add to the powerful iterative MIMO detection method proposed in [10], [11] an inner encoder with code doping to eliminate any error floor. Compared to [9], the receiver is slightly more complex, as the a priori L-values are fed back to the MIMO detector. In addition to the basic method in [10], we adopt the idea from [11] to compute a refined effective noise variance. Moreover, we show that ordinary Gray mapping can be employed. As a consequence, the two main advantages of Gray mapping can be preserved, namely the lower BER for the first few iterations and that no exhaustive optimization of the mapping is necessary.

This paper is organized as follows. In Section II we present the conventional BICM MIMO transmitter, the channel model and the corresponding iterative MMSE receiver. Section III introduces the new transmitter with additional inner encoder and the respective receiver. In Section IV we apply the EXIT chart to optimize the performance of the new scheme. Simulation results and the conclusion follow in Sections V and VI.

II. Transmitter and Receiver

Our approach is based on a BICM MIMO model as depicted in Fig. 1 and the receiver in Figs. 2 and 3.

A. Transmitter

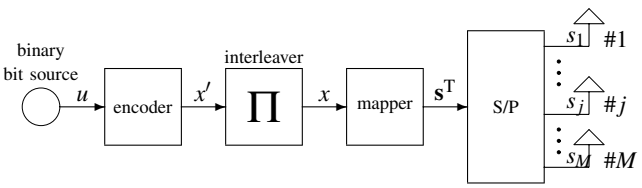

Fig. 1. MIMO transmitter with vertical coding

Boronka, A.; Muhammad, N. S.; Speidel, J.: International Conference on Communications (ICC), Seoul, Korea, May 2005

The transmitter consists of a random binary bit source with output bit-sequence u. The encoder, which operates as an outer encoder applies a systematic convolutional code with rate $R_c = 1/2$. Memory elements and generator polynomials will be discussed later. We use a random interleaver of size $S = 96000$. After encoding, interleaving, and mapping the transmit symbol column vector $\mathbf{s} = (s_1, \ldots, s_M)^T$ is transmitted. M is the number of transmit antennas. Each component s_j is a complex 16-QAM symbol with $Q = 4$ bits per symbol to be sent by antenna j ($j = 1, 2, \ldots, M$) and mean power per symbol E_s per antenna. In [12] this structure was called vertical coding.

B. Channel model and receiver

We use the widely accepted MIMO system model, described by

$$\mathbf{r} = H\mathbf{s} + \mathbf{n} \quad . \tag{1}$$

$\mathbf{r} = (r_1, \ldots, r_N)^T$ is the received symbol column vector, where r_i is the component for antenna i ($i = 1, 2, \ldots, N$) and N is the number of receive antennas. The channel matrix is given by $H = (\mathbf{h}_1 \ldots \mathbf{h}_M)$, where $\mathbf{h}_j = \left(h_{1,j}, \ldots, h_{N,j}\right)^T$ is a column vector of H. The impulse response $h_{i,j}$ from transmitter j to receiver i is modelled as a zero-mean, complex Gaussian random variable satisfying $\mathsf{E}\left\{\left|h_{i,j}\right|^2\right\} = 1$ (i. e. the channel is passive). All entries of H are i.i.d and assumed to be known at receiver side. $\mathbf{n} = (n_1, \ldots, n_N)^T$ is an additive noise column vector with components n_i at receive antenna i, which are complex AWGN, each with zero-mean and variance σ_n^2 ($i = 1, 2, \ldots, N$). This means that real and imaginary part of n_i are Gaussian with variance $\sigma_n^2/2 = N_0/2$ each. We consider $\mathbf{n}$ to be uncorrelated with expected value $\mathsf{E}\{\mathbf{n}\mathbf{n}^*\} = \sigma_n^2 I_N$. I_N is the identity matrix of size N. Furthermore, it is assumed that the vectors $\mathbf{s}$ and $\mathbf{n}$ are uncorrelated, i.e. $\mathsf{E}\{\mathbf{s}\mathbf{n}^*\} = 0$.

We define the SNR to be

$$\mathrm{SNR} = \frac{E_b}{N_0} = \frac{M \cdot E_s \cdot N}{R_c \cdot M \cdot Q \cdot N_0} = \frac{E_s \cdot N}{R_c \cdot Q \cdot \sigma_n^2}, \tag{2}$$

where E_b is the transmitted energy per information bit at the receiver and N_0 the noise power spectral density.

The receiver is depicted in Fig. 2. One branch of the MIMO detector is shown in Fig. 3. For a detailed description and analysis of this model the reader is referred to [10], [11].

In Fig. 2 a shorthand notation is introduced for the L-values, e.g. the a posteriori L-values computed by the MAP demapper $L\left(x_k^{d_\mu} \left| y_{d_\mu}\right.\right)$ are abbreviated by D_1 and so on. As can be seen from Fig. 3, the a priori L-values A_1 for the MIMO detector are being utilized at three instances: First, they are used to reconstruct the expectation value of the symbols that were transmitted from the other antennas and therefor allow for soft interference cancellation. Next, they influence the computation of the MMSE filter vectors, so that further interference supression can be achieved. Finally, they are used by the MAP demapper to update the calculation of the a posteriori L-values D_1.

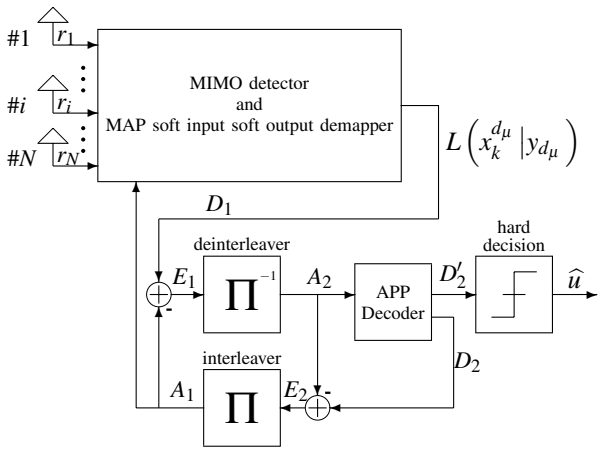

Fig. 2. Receiver structure for iterative detection of a vertical encoded MIMO signal

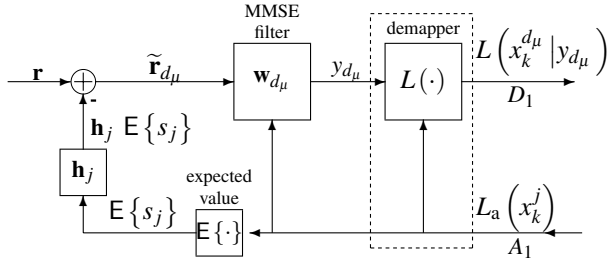

Fig. 3. MIMO detector branch of detection step d_μ

III. Additional Inner Encoder

In Fig. 1 the mapper operates as an inner encoder. To "bend up" its transfer characteristic in the EXIT chart, we combine the mapper with an additional rate 1 inner encoder. It consists of a recursive systematic encoder with memory 1 and code rate $1/2$, followed by a switch as depicted in Fig. 4. The position of the switch depends on $t \bmod P$, where mod is the modulo operator and P is the doping period. Since this

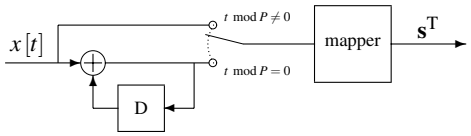

Fig. 4. Additional rate 1 encoder at transmitter

additional encoder has only one memory element, its decoding complexity is small. The recursive encoder takes the bits $x[t]$ from the interleaver and computes parity bits. The switch periodically replaces ("dopes") every P^{th} input bit $x[t]$ by a parity bit. Thus, the code rate is 1. As we will see later, a typical value is $P = 50$. In [13], this scheme was applied with $P = 4$.

At the receiver side, we obviously need an additional inner APP decoder. Furthermore, we have to ensure that all L-values are delivered to the correct device. This can be accomplished by the switches depicted in Fig. 5. This block diagram has to replace the dashed box from Fig. 3. As the additional

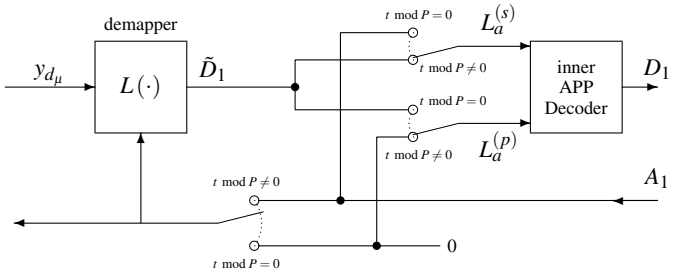

Fig. 5. Changes at the receiver due to additional inner encoder

inner encoder is a rate $1/2$ encoder, which is punctured to rate 1, the inner APP decoder expects a priori L-values for the systematic (undoped) bits $L_a^{(s)}$ and for the parity (doped) bits $L_a^{(p)}$ (indicated by two seperate inputs in Fig. 5). For the undoped bits $(t \bmod P \neq 0)$ the a priori information A_1 stemming from the outer APP decoder in Fig. 2 is fed back to the demapper, the MMSE filter and the expectation builder. The a posteriori L-value from the MAP demapper $\tilde{D}_1$ is forwarded to the systematic input $L_a^{(s)}$, while the value for $L_a^{(p)}$ is set to zero, because no parity bit was transmitted. For $t \bmod P = 0$ the a posteriori L-value $\tilde{D}_1$ corresponds to a parity bit and is therefor directed to the parity input $L_a^{(p)}$. In this case the a priori L-value A_1 must not be fed back to the MIMO detector, because it represents a systematic bit, which was replaced by the respective parity bit. Thus, it is the input value for $L_a^{(s)}$. A similar procedure was used in [8], [9] and the reader may use these references for further study.

IV. Code Design with EXIT Chart

In this section we use the EXIT chart technique to find an appropriate outer code such that the transfer characteristics of outer decoder and the combination of the MIMO detector and additional inner rate 1 decoder are optimally matched. Further, the doping period P is optimized.

A. Original system

First, we investigate the transfer characteristics of the demapper and outer decoder of the original system in [11] with receiver in Figs. 2 and 3 as a baseline. Fig. 6 shows the EXIT chart for Gray mapping and outer decoders with memory 2, 4, 6, and 8 resp. The MIMO system operates with $M = N = 4$ and 16-QAM. For the remainder of this paper we restrict ourselves to this antenna configuration. The encoders with memory 2, 4, 6, and 8 use generator polynomials of (04,07), (023,037), (0147,0117), and (0435,0777) respectively. All polynomials are given in octal numbers. The memory 2 encoder is non-recursive. The transfer characteristic of the demapper is plotted for an SNR of 6 dB in Fig. 6. It can be seen that encoders with small memory yield an intersection point between the curves of Gray demapper and decoder, which is not close enough to the upper right corner $(I_A = 1, I_E = 1)$ of the EXIT chart. This leads to an error floor at high BER. In the considered case, an encoder with more memory can overcome this problem. We will discuss BER in more detail in Section V.

As an example of various anti-Gray mappings given in [1], [9], [14]–[16] we have chosen the modified set partitioning

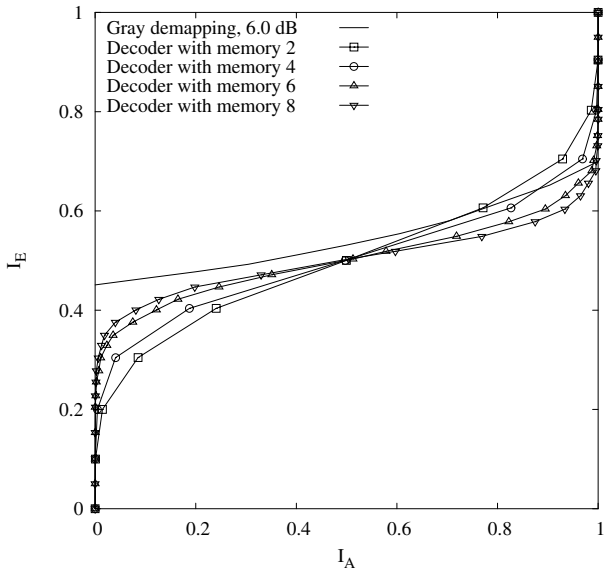

Fig. 6. EXIT chart of 16-QAM Gray demapper, SNR of 6 dB and outer decoders with memory 2, 4, 6, and 8

(MSP). For this mapping, the memory 2 encoder is selected, because it yields the best match to the characteristic of the demapper. Nevertheless, the turbo cliff will be shifted to higher SNR even with a low memory code. On the other hand, the error floor is significantly reduced, because the intersection of the two characteristics is close to the upper right corner of the EXIT chart. This effect can be seen in Fig. 7. It also shows

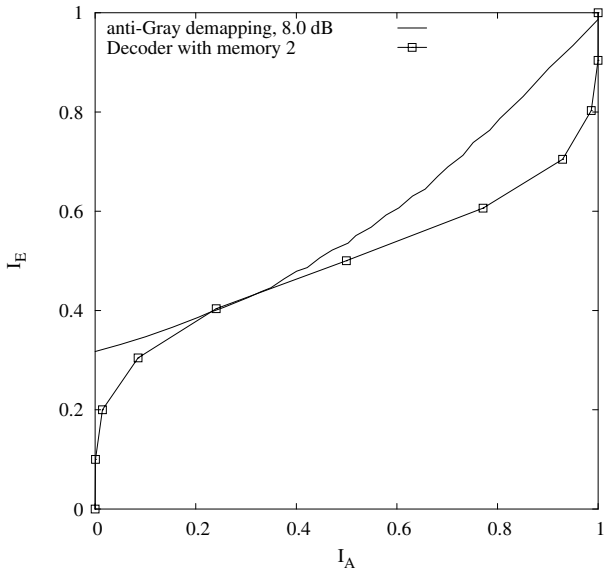

Fig. 7. EXIT chart of demapper with anti-Gray mapping, SNR of 8 dB and outer decoder with memory 2

that there is no tunnel between the curves. Thus, SNR > 8 dB is required for iterative decoding.

B. New scheme with additional inner encoder

Now we investigate the new proposal given by the additional inner encoder with code doping period P and the receiver in

Figs. 2 and 3, where the dashed part in Fig. 3 is replaced by the unit from Fig. 5. Fig. 8 illustrates that the additional

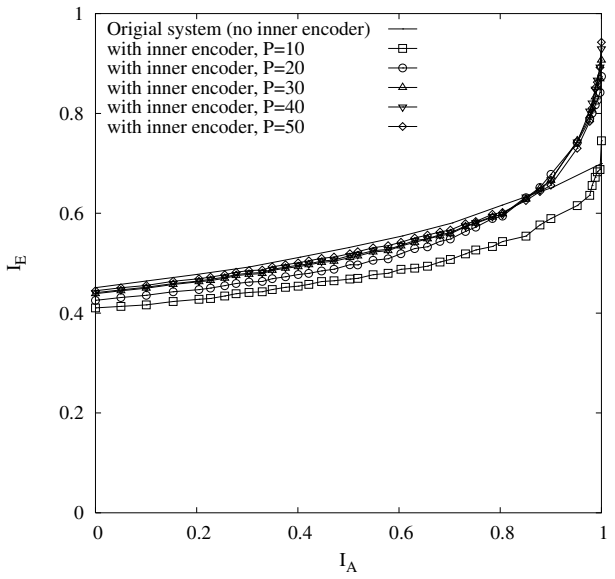

Fig. 8. Transfer characteristics of the combination of Gray demapper with additional inner APP decoder, SNR of 6 dB, and different values of P compared with original system

inner encoder has bent up the characteristics. In detail, the additional inner encoder slightly lowers the curve of the original demapper for $I_A \lessapprox 0.8$, but rises it significantly at the right edge of the EXIT chart. Of course, the actual shape depends on P. It can be seen that the curves for $P = 30$, $P = 40$, and $P = 50$ are quite similar. For the remainder of this paper we select $P = 50$ and search for a matching decoder.

There is no need to investigate the combination of an anti-Gray mapping with additional inner encoder, because the transfer characteristic of the demapper in Fig. 7 already comes close enough to the upper right corner of the EXIT chart. During our simulations we indeed observed that there is no noteworthy improvement with anti-Gray mapping.

For the Gray mapping with additional inner encoder we have selected the outer encoder with memory 6, because of an almost optimal match. The EXIT chart is depicted in Fig. 9. It can be seen immediately that there is no intersection between the two curves for $I_A < 1$ and that there is a tunnel for iterative decoding. Thus, we expect the decoding process to converge for SNR around 6 dB.

V. Simulation Results

We have simulated the BER for the original and the new scheme as a function of SNR. For each simulation 10^7 information bits are used.

A. Original system

Fig. 10 shows the BER of the original system when Gray mapping is used. An outer encoder with memory 6 is applied, as discussed in Section IV. It can be seen that there exists a

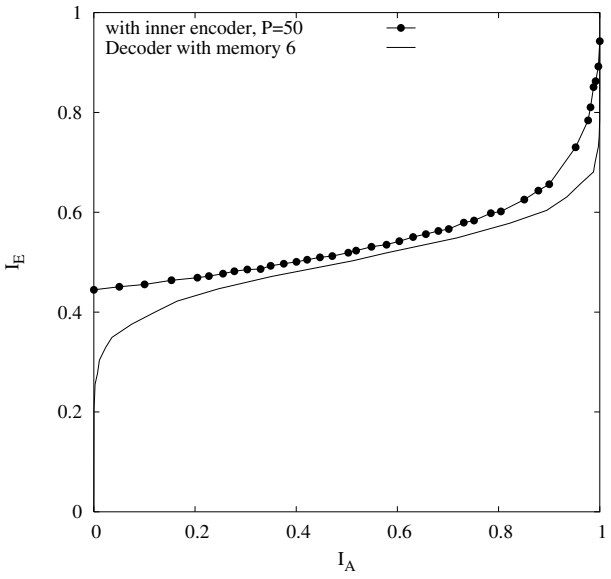

Fig. 9. EXIT chart of the combination of Gray demapper with additional inner APP decoder, SNR of 6 dB, $P = 50$, and a systematic convolutional encoder with memory 6

turbo cliff at about 6 dB. However, the cliff is not very pronounced and the resulting error floor is rather high. This is due to the fact that the intersection of the transfer characteristics of demapper with outer decoder in Fig. 6 is far away from the upper right corner of the EXIT chart. With anti-Gray

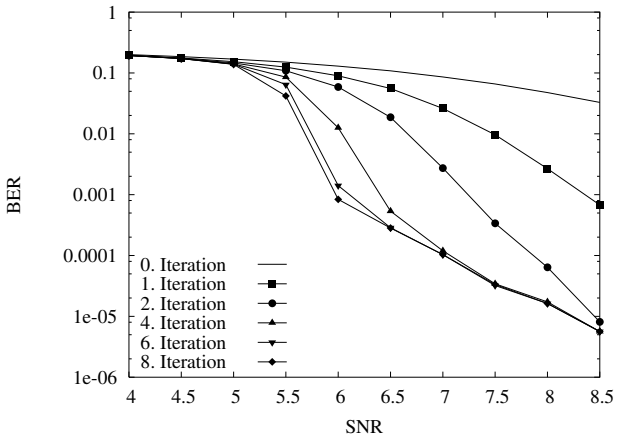

Fig. 10. BER of original system with Gray mapping and a systematic convolutional encoder with memory 6

mapping shown in Fig. 11 the turbo cliff occurs around 8 dB, as predicted by the EXIT chart in Fig. 7. Obviously, this is about 2 dB higher than for Gray mapping. However, with anti-Gray mapping the error floor is significantly reduced.

B. New scheme with additional inner encoder

Fig. 12 shows the BER of the new proposal. It can clearly be seen that we have combined both advantages: an early turbo cliff at about 6 dB and the elimination of the error floor. Furthermore, only 8 iterations are required compared to 14 in Fig. 11. This is due to the fact that the tunnel between the

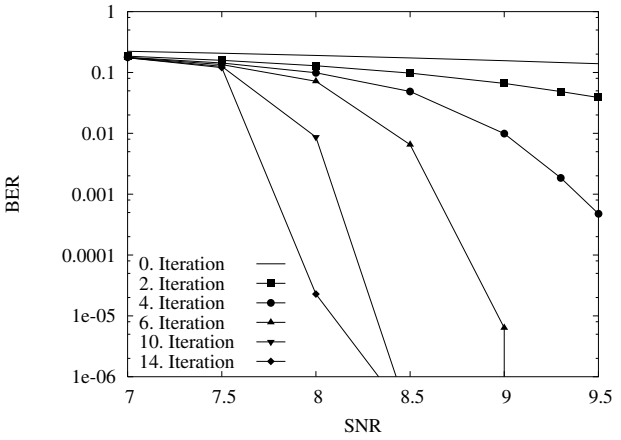

Fig. 11. BER of original system with anti-Gray mapping (MSP) and a systematic convolutional encoder with memory 2

transfer characteristics in Fig. 9 is almost horizontal. It should be noted that an increase of outer encoder memory, e.g. to 6 as in Fig. 12, does not improve the performance shown in Fig. 11. The reason is the matching of the EXIT chart characteristics, discussed in Section IV, which is best for memory 2.

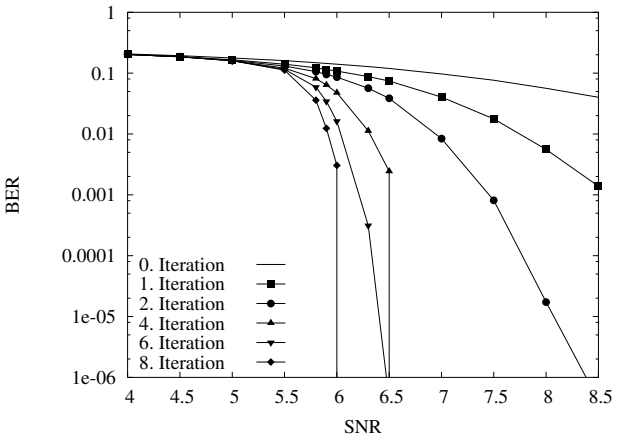

Fig. 12. BER of new scheme with additional inner encoder, Gray mapping, and a systematic convolutional encoder with memory 6

VI. Conclusion

In this paper we have presented an improved scheme for iterative detection of MIMO signals without BER floor. Starting from the solutions given in [10], [11], we have introduced an additional inner encoder. Its code rate was adjusted to 1 by code doping. Thus, no additional bit overhead is required. Doping period P and outer code were optimized by using the EXIT chart. $P = 50$ and an outer recursive systematic convolutional encoder with memory 6, generator polynomials (0147,0117) and rate $1/2$ were selected. For a 4×4 MIMO system with 16-QAM Gray mapping we have completely removed the error floor and shifted the turbo cliff from 8 to 6 dB compared to state of the art. The number of necessary iterations was reduced by about a factor of 2 compared to anti-Gray mapping. At the receiver, decoding complexity is only slightly increased by an additional 2 state inner APP decoder, because we have selected the additional inner encoder with only memory 1.

References

[1] F. Schreckenbach, N. Görtz, J. Hagenauer, and G. Bauch, "Optimized symbol mappings for bit-interleaved coded modulation with iterative decoding," in *IEEE Global Telecommunications Conference (GLOBECOM) 2003*, vol. 6, San Francisco, California, USA, December 1-5, 2003, pp. 3316–3320.

[2] S. ten Brink, J. Speidel, and R.-H. Yan, "Iterative demapping and decoding for multilevel modulation," in *IEEE Global Telecommunications Conference (GLOBECOM) 1998*, vol. 1, Sydney, Australia, November 8-12 1998, pp. 579–584.

[3] G. Caire, G. Taricci, and E. Biglieri, "Bit-interleaved coded modulation," *IEEE Transactions on Information Theory*, vol. 44, no. 3, pp. 927–945, May 1998.

[4] S. ten Brink, "Design of concatenated coding schemes based on iterative decoding convergence," Dr.-Ing. dissertation (Ph.D.), University of Stuttgart, 2001, published at Shaker Aachen, Germany, ISBN 3-8322-0684-1.

[5] S. ten Brink, "Convergence behavior of iteratively decoded parallel concatenated codes," *IEEE Transactions on Communications*, vol. 49, no. 10, pp. 1727–1737, October 2001.

[6] S. ten Brink, "Exploiting the chain rule of mutual information for the design of iterative decoding schemes," in *39th Allerton Conference on Communications, Control and Computing*, Monticello, Illinois, USA, October 3-5, 2001.

[7] F. Sanzi, A. Slama, and J. Speidel, "Multicarrier code division multiplex with iterative MAP symbol-by-symbol estimation," in *IEEE Global Telecommunications Conference (GLOBECOM) 2001*, vol. 2, San Antonio, Texas, USA, November 25-29, 2001, pp. 886–890.

[8] S. Pfletschinger and F. Sanzi, "Iterative demapping for OFDM with zero-padding or cyclic prefix," in *IEEE International Conference on Communications (ICC) 2004*, Paris, France, June 20-24, 2004.

[9] S. Pfletschinger and M. Navarro, "A low complexity MIMO system based on BICM with iterative decoding," in *The 13th IST Mobile & Wireless Communications Summit 2004*, Lyon, France, June 27-30, 2004.

[10] M. Witzke, S. Bäro, F. Schreckenbach, and J. Hagenauer, "Iterative detection of MIMO signals with linear detectors," in *36th Asilomar Conference On Signals, Systems And Computers (ACSSC) 2002*, vol. 1, Pacific Grove, California, USA, November 3-6, 2002, pp. 289–293.

[11] A. Boronka, T. Rankl, and J. Speidel, "Iterative nonlinear detection of MIMO signals using an MMSE-OSIC detector and adaptive cancellation," in *5th International ITG Conference on Source and Channel Coding (SCC) 2004*, Erlangen, Germany, January 14-16, 2004, pp. 17–24.

[12] X. Li, H. Huang, G. J. Foschini, and R. A. Valenzuela, "Effects of iterative detection and decoding on the performance of BLAST," in *IEEE Global Telecommunications Conference (GLOBECOM) 2000*, vol. 2, San Francisco, California, USA, November 27 - December 1, 2000, pp. 1061–1066.

[13] S. Bäro, "Turbo detection for MIMO systems: Bit labeling and precoding," in *5th International ITG Conference on Source and Channel Coding (SCC) 2004*, Erlangen, Germany, January 14-16, 2004, pp. 11–16.

[14] A. Chindapol and J. Ritcey, "Design, analysis, and performance evaluation for BICM-ID with square QAM constellations in Rayleigh fading channels," *IEEE Journal on Selected Areas in Communications*, vol. 19, no. 5, pp. 944–957, May 2001.

[15] J. Tan and G. L. Stüber, "Analysis and design of interleaver mappings for iteratively decoded BICM," in *IEEE International Conference on Communications (ICC) 2002*, vol. 3, New York, USA, April 28 - May 2, 2002, pp. 1403–1407.

[16] A. Boronka and J. Speidel, "A low complexity MIMO system based on BLAST and iterative anti-Gray-demapping," in *The 14th IEEE International Symposium on Personal, Indoor and Mobile Radio Communications (PIMRC) 2003*, vol. 2, Beijing, China, September 7-10, 2003, pp. 1400–1404.